Journal of Marine Science and Technology

Volume 32 | Issue 1 Article 4

Adaptive Prediction Horizon Energy-saving Collision-Free MPC of Ships Based on Ship-Shore Cooperation

Han Xue
College of Navigation, Jimei University, Xiamen 361021,Fujian,China), imlmd@163.com

Enjie Yang
.College of Navigation, Jimei University, Xiamen 361021,Fujian,China

Recommended Citation

Xue, Han and Yang, Enjie (2024) "Adaptive Prediction Horizon Energy-saving Collision-Free MPC of Ships Based on Ship-Shore Cooperation," *Journal of Marine Science and Technology*: Vol. 32: Iss. 1, Article 4.
DOI: 10.51400/2709-6998.2730
Available at: https://jmstt.ntou.edu.tw/journal/vol32/iss1/4

Adaptive Prediction Horizon Energy-saving Collision-Free MPC of Ships Based on Ship-Shore Cooperation

Acknowledgements

This work was supported in part by the National Natural Science Foundation of China (No. 52201411, 62171369) and Natural Science Foundation of Fujian Province (No. 2021J01819, 2023I0019).

RESEARCH ARTICLE

Adaptive Prediction Horizon Energy-saving Collision-Free MPC of Ships Based on Ship-Shore Cooperation

Han Xue*, Enjie Yang

College of Navigation, Jimei University, Xiamen 361021, Fujian, China

Abstract

In order to perform the close association between ship maneuvering control and energy consumption through the control strategy, this paper designs an adaptive prediction horizon based energy-saving robust nonlinear model predictive control (APHERNMPC) for underactuated ships to deal with the actual control and state constraints during berthing based on ship-shore cooperation. An improved Emperor Penguin Optimizer (EPO) method is proposed for collision avoidance decision. To solve the problems of falling into local optimum and reducing the convergence speed, the traditional EPO is improved based on Sobol sequence in order to enhance the diversity and ergodicity of the population. The multi-ship encounter situation is tested based on ship-shore cooperation. The results show that the consumed energy increases with the increase of the speed. In addition, when the intensity and direction of the environmental disturbance are different, the energy consumption is also different. The energy consumed by the ships when moving at different speeds and in different environmental intensities is discussed. Furthermore, the reasons for the fluctuations in energy consumption with respect to the ship speed are analyzed.

Keywords: Underactuated ships, Model predictive control, Berthing control, Energy-saving, Ship collision avoidance, Ship-shore cooperation

1. Introduction

1.1. Research background

With the increasing demand for energy and the dual constraints of the environment and the survival of enterprises, the energy conservation and emission reduction of ships have been widely studied. In previous studies, the energy consumption was rarely considered in path planning. The water area at the wharf apron is a restricted zone, and the traffic flow of nearby ships is more complex, which greatly increases the difficulty and risk of berthing. Therefore, to develop the unmanned ship technology and improve the safety of berthing, studying the automatic berthing control is crucial. Although a great progress has been made in ship collision avoidance and control, the following problems still exist:

(1) The energy devices that can be carried by unmanned ships are limited. In addition, it is important to improve the endurance of these ships in order to consider the energy consumption as one of the goals in control algorithms. Moreover, most of the collision avoidance and control algorithms do not consider the energy consumption.
(2) It may be difficult to deal with the identity conflict in multi-ship encounter situations. Most of the studies on collision avoidance decision-making focus on the collision avoidance

Received 28 August 2023; revised 17 December 2023; accepted 21 December 2023.
Available online 11 March 2024

* Corresponding author.
E-mail address: imlmd@163.com (H. Xue).

https://doi.org/10.51400/2709-6998.2730

opportunity in the case of give-way ships, while less studies are conducted on the stand-on ships.

Therefore, it is very important to develop new collision avoidance control mechanisms and algorithms. This has a theoretical significance for ship control.

1.2. Related work

Nowadays, ship berthing control has been considered as one of the most challenging tasks. In a recent study on ship auto berthing control [1], a virtual navigation system, based on heuristic dynamic programming, was used to investigate the berthing control of automatic ships. A robust neural network was proposed to reconstruct the lumped uncertainties [2]. An asymmetric barrier Lyapunov function-based fixed-time ship berthing control was also proposed [3]. The underactuated ship method, based on nonlinear model predictive control, provided the optimal rudder angle and propeller speed to perform the automation of the ship docking process [4]. An automatic parking control strategy for 3 degree of freedom (DOF) underactuated surface vehicles, based on concise backstepping, was proposed [5]. Finally, a control method of autonomous docking and undocking was proposed using the adaptive mutated beetle swarm prediction algorithm [6]. However, most of these studies only assume a simple berth without the spatial constraints of the restricted waters of the wharf, while actual control and state constraints exist during berthing.

Model predictive control (NPC) is an efficient method for ship berthing control, which allows to solve this problem [7]. In the ship motion control field, the model predictive controller was used to generate a reference tracking speed that satisfies the constraint [8]. An auxiliary time-varying tracking controller was constructed in the nonlinear model predictive control framework to assist the terminal constraint design [9]. A NPC scheme was proposed to track an underactuated ship with only two available controls: the ship surge force and its yaw moment [10]. A two-layer recurrent neural network was used to iteratively solve the reconstructed minimax optimization problem. In addition, a data-driven predictive control method was proposed [11]. A nonlinear model predictive controller for ship path tracking, under regular waves, was also presented in [12]. The study presented in [13] designed such controller for the vertical motion attenuation of passenger ships under irregular wave excitation. Moreover, an event triggered nonlinear model predictive control solution was developed using the trajectory tracking of underactuated ships [14]. Finally, a robust nonlinear model predictive control scheme was proposed for the dynamic positioning of ships that are affected by time-varying environmental disturbances and input saturation [15]. However, most of the studies presented in this literature review aim at tracking a predetermined reference trajectory with adjusting control gain. This will lead to considerable energy consumption. However, in the existing studies, the ship maneuvering control and energy-saving are always independently analyzed, and thus their close correlation is often neglected.

Studies on fuel consumption and ship motion control algorithms have been recently emerged. For instance, Li [16] proposed a nonlinear switching feedback technology. The model predictive control was used to improve the fuel efficiency and power system stability [17]. The second order closed-loop gain shaping controller had energy-saving effect and smoothness [18]. The energy consumption was considered during the control of underactuated ships [19]. Moreover, using the simulation data of irregular wave field, a circular path tracking analysis of the designed controller was conducted, and the tracking performance and energy consumption were compared with those of the traditional control method [20]. Osman and Nuri [21] estimated the accurate volume of liquid while considering the trim and heel conditions of the ship.

The swarm intelligence algorithms, such as the Emperor Penguin Optimizer (EPO), are useful for ship collision avoidance. Dhiman [22] proposed an EPO for solving engineering problems. Baliarsingh [23] analyzed the high-dimensional biomedical data using an evolutionary multi-objective EPO. Ganesh [24] developed a modified EPO method for the optimal allocation that concerns energy storage systems and phasor measurement units. Khalid [25] comprehensively reviewed the existing EPOs. Khan [26] studied the recycling waste classification using the EPO. Lu [27] discussed a converged EPO for bidding strategy in a day-ahead deregulated market clearing price in China. Kaur [28] designed a multi-objective EPO for global optimization. Dhiman [29] studied a binary EPO for automatic feature selection. Xing [30] improved the EPO based multilevel thresholding for color image segmentation. Although the above methods could improve the algorithm performance, they require a complex and large-scale change, which causes a great limitation in terms of computational load and cost in practical applications. Therefore, this study improve the efficiency of energy saving while ensuring the accuracy and safety of the path following.

1.3. Contributions

This study aims at adaptively selecting an appropriate prediction horizon for energy-saving, and using EPO to select the turning angle for collision avoidance in order to determine the desired vessel course at the next moment. The relationship between collision avoidance and NMPC is summarized as follows: the collision avoidance method based on EPO designs an appropriate trajectory and course similar to those of the MPC. This paper aims at bridging the gap between manipulation control and energy saving. Its main contributions are summarized as follows:

(1) A novel energy-saving adaptive-prediction-horizon model predictive control is designed. The close association between ship maneuvering control and energy consumption is performed using the control strategy. The asymptotic stability of the system is proved.
(2) An improved EPO method is proposed. To solve the problems of falling into local optimum and reducing the convergence speed, the traditional EPO is improved based on Sobol sequence where a quasi-random sampling method is introduced in the initialization stage to enhance the diversity and ergodicity of the population.
(3) A ship-shore cooperation method is proposed. The multi-ship encounter situation is studied by analyzing the effect of the ship-shore cooperation under different combination modes based on ship maneuverability and collision avoidance rules.

2. Preliminaries and problem statement

2.1. Emperor penguin optimizer

The EPO is a swarm intelligent optimization algorithm developed by Dhiman and Kumar in 2018 [22]. It consists in simulating the behavior of emperor penguins crowding together for heating during the winter semester. It has few parameters and high convergence accuracy. When the bad weather comes, the penguins will huddle together to keep out wind and cold conditions. The emperor penguins gather to warm each other in the Antarctic extreme winter when the temperature reaches −40 °C. To stay warm, all the penguins make equal contribution, their social behavior is extremely united, and the labor partitioning is clear.

The algorithm consists of setting the position range selected in the process of emperor penguin curling up for heating within the mesh range of polygon. In the gathering process, each emperor penguin is adjacent to at least two others, and the selection of neighbors is random. In the emperor penguin clustering process, the range boundary is an irregular polygon. The gradient γ of the wind around the emperor penguin cluster is used to represent the boundary of the whole cluster, and the wind speed is denoted by α. Its gradient is given by:

$$\gamma = \Delta\alpha \tag{1}$$

where μ represents the polygon plane function, i represents the imaginary constant, and β represents the complex plane ordinate of the polygon boundary that the penguin moves to.

A complex potential is reached by integrating vector β with the wind speed α:

$$\mu = \alpha + \mathrm{i}\,\beta \tag{2}$$

The wind speed and cluster boundary can be presented by Eqs. (1) and (2), respectively.

The harsh environment in the Antarctic allows the emperor penguins to stay warm by gathering in cold weather during migration. If the current gathering radius (d) is greater than 0.5, its temperature (W) is equal to zero. However, when d is smaller than 0.5, W is equal to 1. The temperature gradient curve $\overline{W}$ can be expressed as:

$$\overline{W} = W - \frac{t_{\max}}{x - t_{\max}} \tag{3}$$

where $t_{\max}$ is the maximum number of iterations, x is the current number of iterations, and temperature W is given by:

$$W = \begin{cases} 0, & d \geq 0.5 \\ 1, & d < 0.5 \end{cases} \tag{4}$$

The distance between the emperor penguins within the cluster is expressed as the distance between the individual and the one in the center of the cluster. The cluster distance is expressed as:

$$L_{ep} = \left\| F(\Gamma) O_{best}(x) \text{-} I O_{ep}(x) \right\| \tag{5}$$

$$\Gamma = B_{move}(W + P_{acc}) Random() - \overline{W} \tag{6}$$

$$P_{acc} = \left\| O_{best}(x) \text{-} O_{ep}(x) \right\| \tag{7}$$

$$I = Random([0, 1]) \tag{8}$$

$$F = \xi e^{-\frac{x}{\varphi}} - e^{-x} \tag{9}$$

where L_{ep} denotes the distance from the emperor penguin to the center, x represents the current number of iterations, Γ and I form the vector of

influence factors used for defining the emperor penguin volume to avoid conflicts between individuals, $O_{best}(x)$ is the optimal solution in the x iteration, $O_{ep}(x)$ represents the position vector of the current emperor penguin, F represents the social status of the emperor penguins allowing to distinguish between the best individuals and the ordinary ones, B_{move} is the moving step size which can be set to 2.5, P_{acc} represents the precision of polygon mesh by comparing the difference with the best, ξ and φ are control parameters in the ranges of 2−3 and 1.5−2, respectively.

The individual in the emperor penguin cluster updates the location information by moving to the direction of the one in the cluster center. The location update formula is expressed as:

$$O_{ep}(x+1) = O_{best}(x) - \Gamma L_{ep} \tag{10}$$

where $O_{ep}(x+1)$ represents the next generation update position of the emperor penguin.

In the iteration process, once the mover is relocated, the above parameters of the emperor penguin are recalculated.

2.2. Sobol sequences

The Sobol sequence is a kind of quasi-random sequences, as shown in Fig. 1. The method of sampling the Sobol sequence is more uniform than that of sampling the uniformly distributed random sequence.

There is a quasi-random number sequence flaw in the current. That is, the sample distribution is inconsistent with the real distribution. This mainly occurs in the following two situations: high sampling cost with small number of samples and high space dimension. The quasi-random sequence, also known as low difference sequence, is used to replace the uniformly distributed random sequence. The Sobol random sequence is an example of this kind of sequences. It has high distribution uniformity and low time consumption. Fig. 1(a) shows a scatter plot based on the Sobol random sequence where the mutual overlap is eliminated. This presents a uniform distribution based on the sequence of pseudo random numbers, where some points overlap with each other due to randomness, as shown in Fig. 1(b).

2.3. Collision avoidance

The velocity is denoted by $v_o = (v_{ox}, v_{oy})$, and that of the target ship is denoted by $v_T = (v_{Tx}, v_{Ty})$. The relative speed is computed as [31,32]:

$$v_{OT} = \sqrt{(v_{Tx} - v_{ox})^2 + (v_{Ty} - v_{oy})^2} \tag{11}$$

The relative course is expressed as:

$$\varphi_R = \arctan\frac{v_{Ty} - v_{oy}}{v_{Tx} - v_{ox}} + \alpha_0 \tag{12}$$

where α_0 is computed as:

$$\alpha_0 = \begin{cases} 0, & v_{Bx} \geq v_{Ax}, v_{By} \geq v_{Ay} \\ 180, & v_{Bx} < v_{Ax}, v_{By} \geq v_{Ay} \\ 180, & v_{Bx} < v_{Ax}, v_{By} < v_{Ay} \\ 360, & v_{Bx} \geq v_{Ax}, v_{By} < v_{Ay} \end{cases} \tag{13}$$

where R_T denotes the distance, (φ_A, λ_A) represents the position, (φ_B, λ_B) is the position of the target ship, and α_T is the azimuth which can be computed as:

$$\alpha_T = \arctan\frac{\varphi_B - \varphi_A}{\lambda_B - \lambda_A} + \alpha \tag{14}$$

The absolute value of the difference between the azimuth α_T and the relative course φ_R is given by:

$$\theta = |\varphi_R - \alpha_T| \tag{15}$$

The distance to closest point of approach (DCPA) is computed as:

$$DCPA = R_T \sin\theta \tag{16}$$

The time to the closest point of approach (TCPA) is given by:

$$TCPA = \frac{R_T \cos\theta}{v_{OT}} \tag{17}$$

The conditions of ship encountering are defined as:

$$\begin{cases} 0 \leq DCPA \leq 0.5nm \\ v_{OT} \geq 4 \end{cases} \tag{18}$$

The ship motion is summarized in Fig. 2 [33].

2.4. Mathematical model of under-actuated USV

η, υ, u, v, r, x, y, and Ψ are the position and attitude vector, velocity vector, surge velocity, sway velocity, yaw velocity, surge position, sway position, and yaw angle, respectively, as shown in Fig. 3. The mathematical model of this motion is given by [34]:

$$\dot{\eta} = R(\Psi)\upsilon \tag{19}$$

$$\eta = [x \quad y \quad \Psi]^T \tag{20}$$

$$\upsilon = [u \quad v \quad r]^T \tag{21}$$

where R is the rotation matrix:

$$R=\begin{bmatrix}\cos\Psi & -\sin\Psi & 0\\ \sin\Psi & \cos\Psi & 0\\ 0 & 0 & 1\end{bmatrix} \tag{22}$$

The dynamic models of underactuated ships can be calculated as:

$$\begin{cases}\dot{x}=u\cos\Psi-v\sin\Psi\\ \dot{y}=u\sin\Psi+v\cos\Psi\\ \dot{\Psi}=r\end{cases} \tag{23}$$

The velocity equation can be expressed as:

$$\begin{cases}\dot{u}=\dfrac{m_{22}}{m_{11}}vr-\dfrac{d_{11}}{m_{11}}u+\dfrac{F_{wx}+F_{cx}+\tau_u}{m_{11}}\\ \dot{v}=-\dfrac{m_{11}}{m_{22}}ur-\dfrac{d_{22}}{m_{22}}v+\dfrac{F_{wy}+F_{cy}}{m_{22}}\\ \dot{r}=\dfrac{m_{11}-m_{22}}{m_{33}}uv-\dfrac{d_{33}}{m_{33}}r+\dfrac{N_w+N_c+\tau_r}{m_{33}}\end{cases} \tag{24}$$

where $\tau\ u$ denotes the control input along the surge direction, $\tau\ r$ represents the control input along the yaw direction, m_{11}, m_{22}, and $m33$ respectively represent the first, second, and third elements on the diagonal of the inertia matrix, $d11$, $d22$, and $d33$ are respectively the first, second, and third elements on the diagonal of the linear hydrodynamic damping parameter matrix, X denotes the position and speed vector, Fwx and Fwy are respectively the wind disturbances along the surging and swaying directions, Nw and Nc are respectively the wind and current disturbances along the yawing direction, Fcx and Fcy are respectively the current disturbances along the surging and swaying directions.

2.5. Error dynamics of under-actuated USV

The desired position and speed vector is denoted by Xd. The components of this vector are shown in Eq. (26).

$$X=[x\quad y\quad \Psi\quad u\quad v\quad r]^T \tag{25}$$

$$X_d=[x_d\quad y_d\quad \Psi_d\quad u_d\quad v_d\quad r_d]^T \tag{26}$$

$$\begin{aligned}X_e&=[x_e\quad y_e\quad \Psi_e\quad u_e\quad v_e\quad r_e]^T\\ &=[R\quad I_3]^T(X-X_d)\end{aligned} \tag{27}$$

$$U=[\tilde{\tau}_u,\tilde{\tau}_r]^T \tag{28}$$

where x_d and y_d are respectively the desired surge and sway positions, Ψ_d, u_d, v_d, and r_d are the desired yaw angle, surge speed, sway speed, and yaw angle speed, respectively.

Let Xe, xe, ye, $\Psi\ e$, ue, ve, and re respectively denote the errors of the position and speed vector, surge position, sway position, yaw angle, surge speed, sway speed, and yaw angle, the error dynamics can then be written as:

$$\begin{cases}\dot{x}_e=r_e y_e+r_d y_e+u_e+(1-\cos\Psi_e)u_d-v_d\sin\Psi_e\\ \dot{y}_e=-r_e y_e-r_d y_e+v_e+\sin\Psi_e u_d+(1-\cos\Psi_e)v_d\\ \dot{\Psi}_e=r_e\\ \dot{u}_e=\dfrac{m_{22}}{m_{11}}(v_e r_e+v_d r_e+v_e r_d)-\dfrac{d_{11}}{m_{11}}u_e+\dfrac{1}{m_{11}}\tilde{\tau}_u\\ \dot{v}_e=-\dfrac{m_{11}}{m_{22}}(u_e r_e+u_e r_d+u_d r_e)-\dfrac{d_{22}}{m_{22}}v_e\\ \dot{r}_e=\dfrac{m_{11}-m_{22}}{m_{33}}(u_e v_e+u_e v_d+u_d v_e)-\dfrac{d_{33}}{m_{33}}r_e+\dfrac{1}{m_{33}}\tilde{\tau}_r\end{cases} \tag{29}$$

The proof of Eq. (29) is shown in Appendix A.

3. Main results

The architecture of the proposed algorithm is illustrated in Fig. 4.

3.1. Adaptive prediction horizon in MPC with energy-saving

The prediction horizon, N_p, refers to the length of time to be predicted. As the prediction horizon increases, the system's stability time also increases. The increase in the prediction horizon of the controller also leads to an increase in the solution time, while an excessively small prediction horizon may result in insignificant predictive effects. Meanwhile, an appropriate prediction horizons is necessary guarantee closed-loop stability. There is a significant difference in the control effectiveness between short-term prediction domain and long-term prediction domain.

In this work, a dynamic and adaptive method for adjusting the prediction horizon is designed to balance the control performance and response velocity. A large value of the prediction horizon at the beginning stage can improve the tracking performance of the controller. At the ending stage, decreasing the value of the prediction horizon can reduce the computational complexity of the controller's solution. Compared to traditional control strategies, The method proposed can balance both dynamic and steady-state characteristics. This has certain theoretical guidance significance for

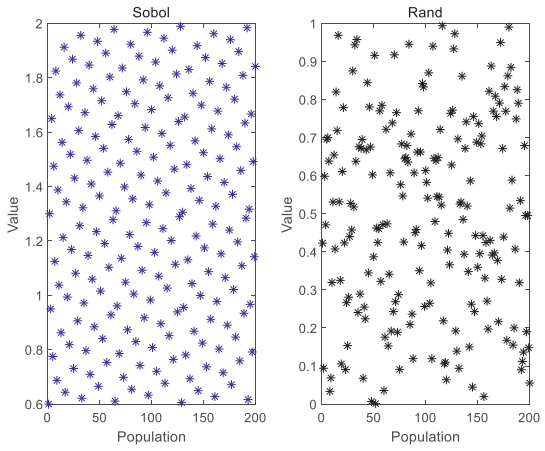

Fig. 1. Sobol sequence.

improving dynamic control performance. The system's dynamic performance has been improved, while maintaining good steady-state performance, greatly reducing the influence of the fixed length of the prediction horizon on control effectiveness.

Therefore, an adaptive prediction horizon MPC is proposed to ensure a high closed-loop stability, reduce the time for the system to enter the terminal set, and thus achieve the desired performance:

$$N_p = \min\left\{N_{p\,\min} e^{\|X_e\|}, N_{p\,\max}\right\} \tag{30}$$

The energy consumption model of the unmanned surface vehicle is introduced into the dissipation function of the objective function.

The control goal is to design the control law and ensure that all the signals are stable and energy-efficient. The objective function minimizes the distance between the position of the ship in the prediction interval and the corresponding point on the reference trajectory, as well as the amount of the control input which is positively correlated with variable the energy consumption.

The discrete system model can be modeled as below:

$$X_{e,k+1} = f(X_{e,k}, U_k) \tag{31}$$

Denote

$$P_k = \|X_{e,k}\|_Q^2 + \|U_{e,k}\|_O^2 \tag{32}$$

where Xe,k is the error state of the system at time k. Ue,k, Q and O are the input of the system at time k, weighting matrix of the error state, and weighting matrix of the input, respectively.

The objective function of the ship in the MPC constrained optimization problem is set at the current k as:

$$J_k = \sum_{i=1}^{N_p} \left(\frac{i}{N_p}\right)^n P_k \tag{33}$$

where n is an integer.

Assumption 1. There exists >0 such that

$$P\big(f(X_e, U)\big) - P(X_e) \le -\beta(X_e) \tag{34}$$

for a positive definite function β satisfying

$$\beta(X_e) \ge \mu P(X_e), \mu > 0 \tag{35}$$

Lemma 1 [35]. Consider the system $x(k+1) = f(x(k))$. If there exists a positive definite bounded function $V(x)$ such that $V(0) = 0$ and for any $x \neq 0$, $V(x) > 0$, in the vicinity of the equilibrium point $x=0$, $V(x)$ is continuous, and $V(x(k+1)) - V(x(k)) \le -\alpha(||x(k)||)$, where α is a class K function, then the system is asymptotically stable.

Theorem 1. For the closed-loop dynamics (31), the state $X_e=0$ is asymptotically stable.
The proof of Theorem 1 is shown in Appendix B.
The framework of Net-MPC is illustrated in Algorithm 1.

Algorithm 1: Framework of Net-MPC

Input: the reference trajectory and the initial state $X_d(0)$
Output: the control strategy
1 Generate the prediction time domain T_p and the sampling interval of MPC
2 while the termination condition is not met do
3 Calculate the objective function in MPC using Eq. (33)
4 Set the state and input of the MPC
5 Solve the MPC optimization problem at t_k
6 Obtain the optimal control sequence predicted at t_k
7 Update the prediction horizon using Eq. (30)
8 Construct the MPC constrained optimization problem at the new sampling time
9 Coastal monitoring of whether there is a risk of collision for vessels
10 Use EPO for collision avoidance until it converges to the optimal solution
11 The shore assigns the priority, and the ships communicate and share their new strategy decisions and predictions
12 end while

3.2. Ship-shore cooperation

The intelligent ship system has been developed from single ship intelligence to a new form of intelligent shipping based on ship-shore collaboration. Through the intelligent equipment on board, the information integration platform relies on data

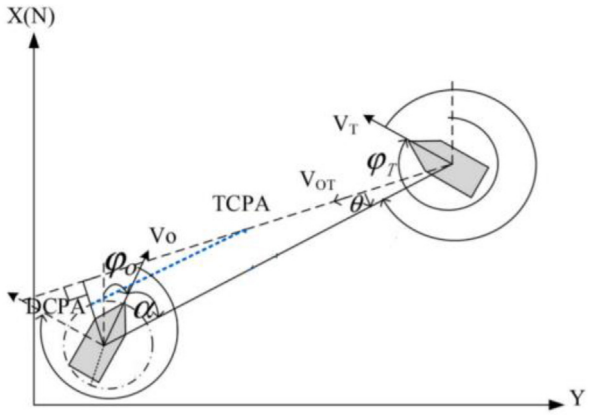

Fig. 2. Relative motion of ships.

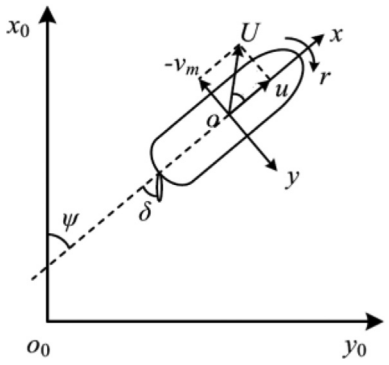

Fig. 3. Model of the ship motion.

related services to perform ship-shore information communication, and thus improve the efficiency, economy, and security of the ship operations. The navigation system based on ship-shore collaboration can provide information service and mutual

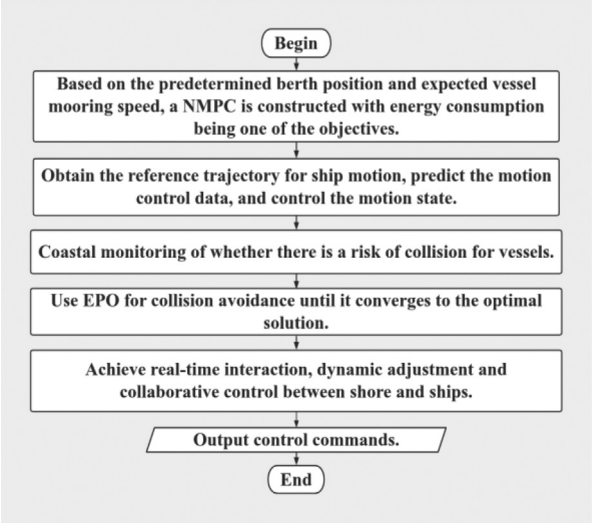

Fig. 4. Method architecture.

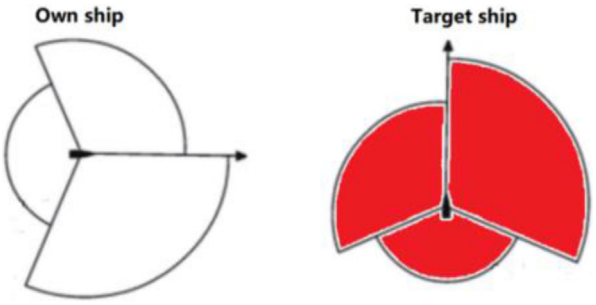

Fig. 5. Non-convexity of collision restraint using Goodwin's ship domain.

collaboration enhancement, in order to optimize the ship-shore resource allocation, improve the reliability of ship navigation, and reduce the associated costs.

The shore control center monitors whether the ships are in danger of collision by analyzing and processing the fusion data. If there exists a danger of collision, it generates collision avoidance instructions according to the navigation conditions of the ships, and sends them instructions of collision avoidance, so that they can control their own course and speed and optimize their local routes. The core of the ship-shore collaboration consists in conducting an integrated and systematic decision system, and optimizing the allocation and balance of information resources between the ship and shore. It emphasizes the real−time interaction and dynamic adjustment between the shore and ship, and performs the reasonable division of labor and cooperative control between the ship and shore.

In the cooperative distributed architecture, each ship has its own controller, which considers its own interests and those of other ships, as well as the

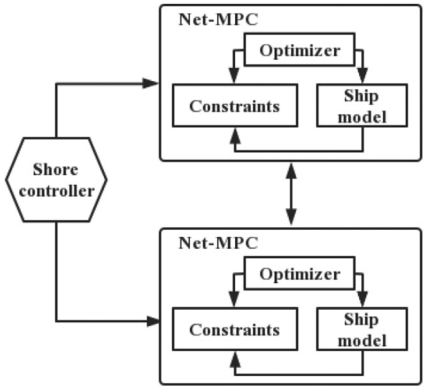

Fig. 6. Framework of priority-based networked energy-saving nonlinear MPC.

dynamic changes around ships. Each ship should communicate and exchange its current measured or estimated state, the predicted reference trajectory, the model parameters, and the time stamp of each sampling state with other ships in an encounter situation. The ships send new predictions to each other, and share the future status and position of other ships.

Fig. 5 illustrates an example of the non-convexity of collision constraint using the Goodwin's ship domain [36], which is composed of three unequal areas of sectors. In this figure, the white area is the feasible movement set of ships while the red one is the infeasible motion set, that is non-convex. The method solves the non-convex optimization problem at each sampling time. The non-convexity is derived from the non-convex feasible set formed by the collision avoidance constraint.

The designed distributed policy update mechanism allows the efficient functioning. The framework of priority distributed predictive control integrates the decentralization of the sensing access strategy of sensors and the model predictive control algorithm, by designing access threshold and priority mechanisms, based on the prediction sequence.

The framework of the priority-based networked energy-saving controller is shown in Fig. 6.

In the above framework, the shore controls several ships. Each ship is equipped with a Net-MPC which consists of an optimizer, ship model, control objective, and constraints. When the ship is sailing normally, the course controller controls it to follow the established path, and calculates the collision risk in real-time using the collision risk model according to its motion information and those of the other ships. When the collision risk is higher than the threshold, the ship enters the collision avoidance state. The collision avoidance course is calculated. The MPC method is then used to control the ship to avoid collision and turn, so as to ensure its navigation safety.

3.3. Collision avoidance based on improved EPO

When a collision is detected, the sequence is determined according to the reference trajectory of the ship and the DCPA of the other ships [37]. Let x_1 and $x2$ respectively denote the turning angle and recovery time, the population fitness, based on the five already described parameters, is then defined as [38]:

Table 1. Parameters of the ships.

Parameter	Value
Length	4.88 m
Beam	2.44 m
Maximum thrust force	400 N

Table 2. Motion parameters of multiple ships.

Ship	x/m	y/m	Course/°	Speed/kn
Ship 1	0	0	45	12
Ship 2	−3143	11,000	105	11
Ship 3	11,786	1309	289	14

$$f = w_1\frac{1}{1+DCPA} + w_2 v x_2 \sin x_1 + w_3(x_1 - 30) + w_4\frac{1}{1+TCPA} \tag{36}$$

where $w1$, $w2$, $w3$, and $w4$ are the weights.

A quantum particle swarm, based on the Sobol random sequence, is introduced in the EPO to increase the population diversity. Let [$x$min, $x$max] the range of the optimal solution, the random number kn ∈ [0, 1], generated by the Sobol sequence, is applied as follows:

$$x_n = x_{min} + k_n(x_{max}\text{-}x_{min}) \tag{37}$$

The Sobol sequence is first used to initialize the population in order to ensure its diversity. Afterwards, when particles fly over the boundary and fly out of the search domain, the diversity of the population decreases with the increase of the number of particles at the boundary, which will affect the global search ability of the algorithm. Therefore, boundary mutation is applied to the particles. A random number produced by the Sobol sequence is used. After this processing, the diversity of the population is increased to reach a greater extent. Thus, the global search ability of the algorithm is improved.

The calculation of the appropriate steering angle avoids the collision, as each ship will leave its original reference track as less as possible. In case of imminent collision, it is necessary to keep a track to avoid collision, and the deviation between the new track and the reference track should be as small as possible. After collision avoidance, the ships return to the original reference track. The control objective can only be achieved through collective behaviors, and the feasible state set of each ship is a function of its own and other ship states.

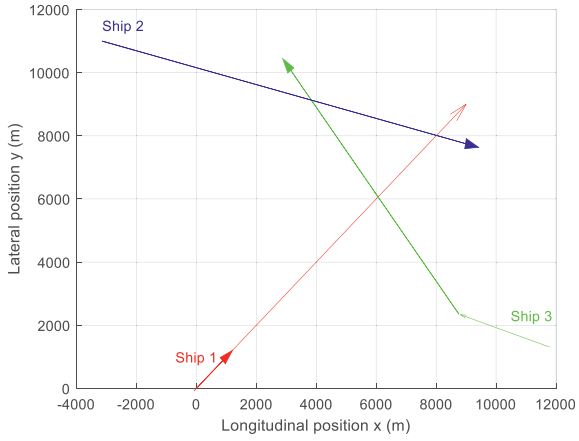

Fig. 7. Encounter situation and collision avoidance results of the three ships.

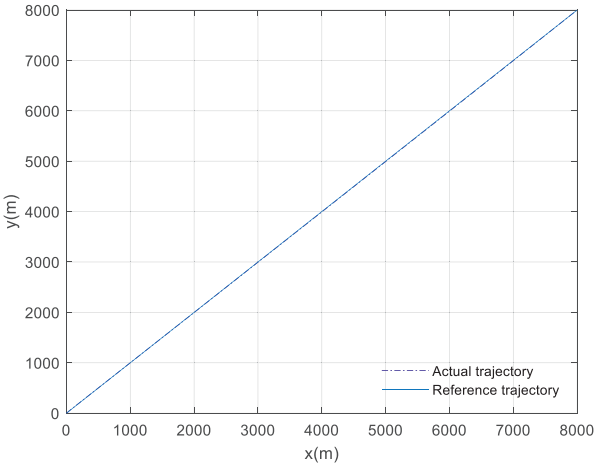

Fig. 10. Motion curve of ship 1.

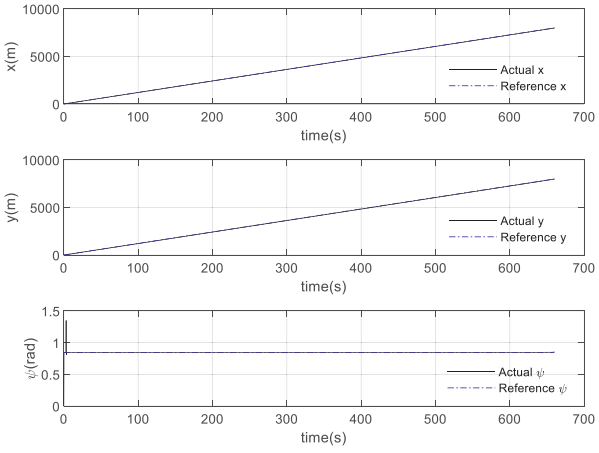

Fig. 8. Surge and sway positions as well as yaw angle curve of ship 1.

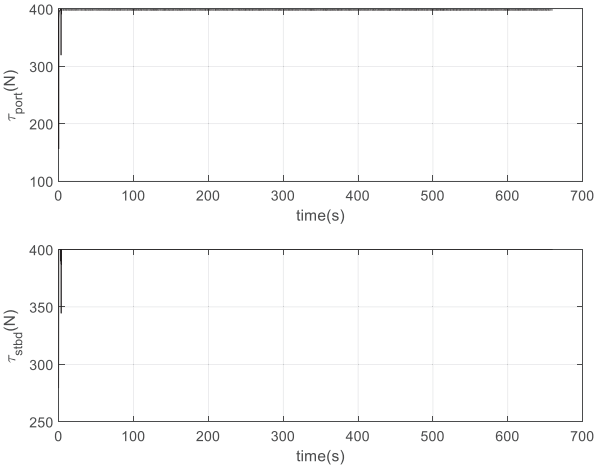

Fig. 11. Control input curve of ship 1.

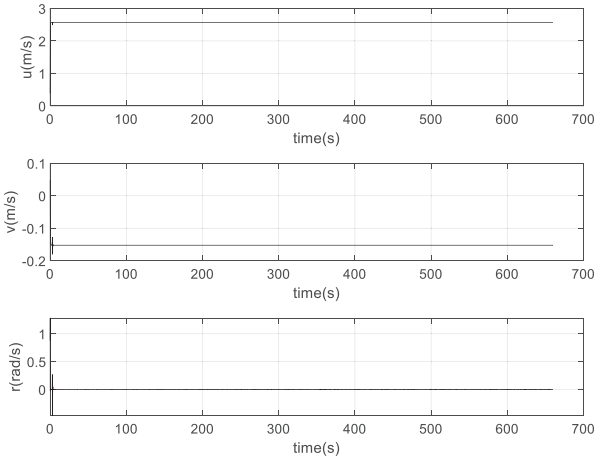

Fig. 9. Speed of ship 1.

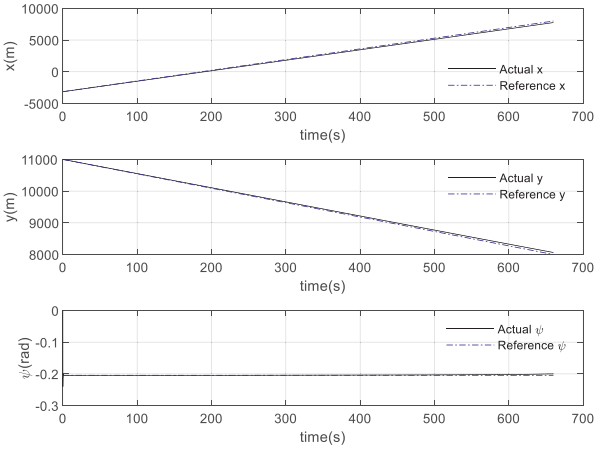

Fig. 12. Surge, sway position and yaw angle curve of ship 2.

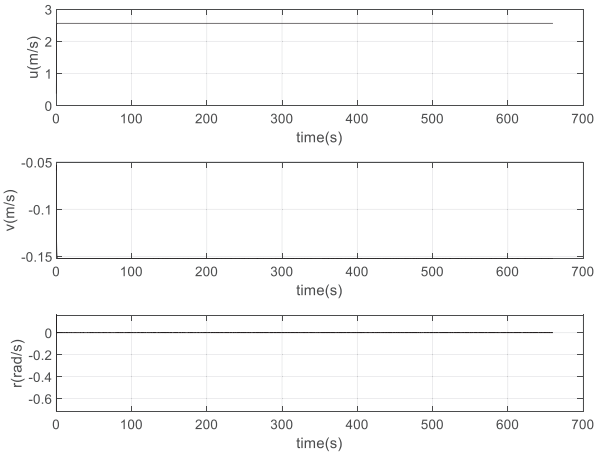

Fig. 13. Speed curve of ship 2.

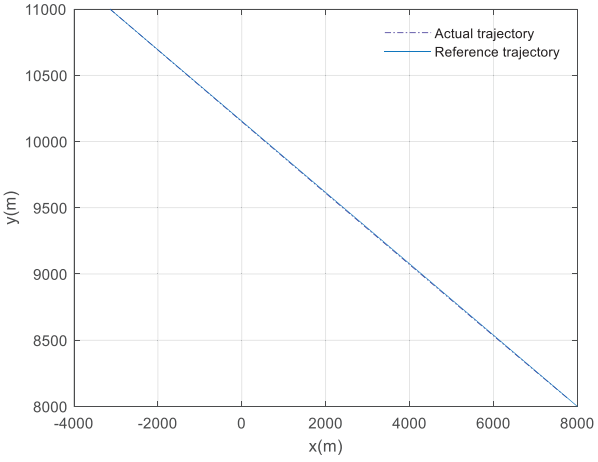

Fig. 14. Motion position of ship 2.

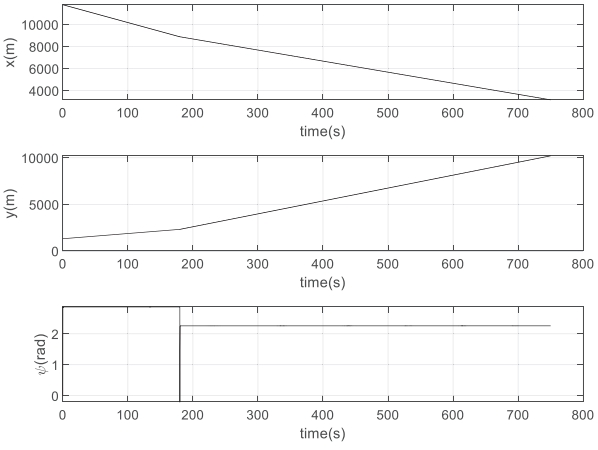

Fig. 15. Surge, sway position and yaw angle curve of ship 3.

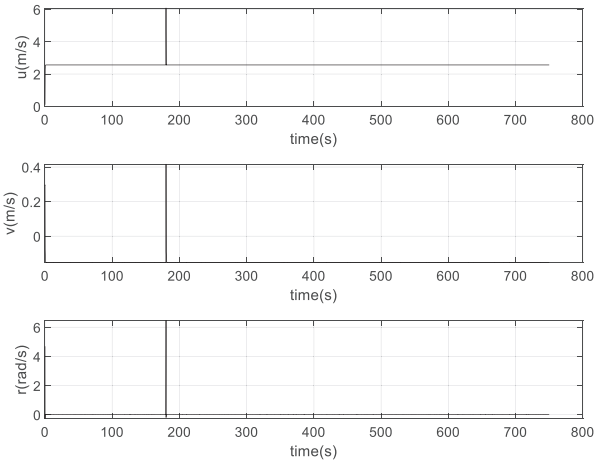

Fig. 16. Speed curve of ship 3.

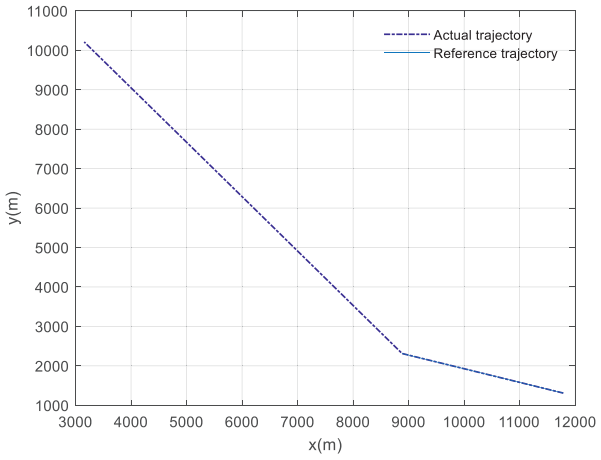

Fig. 17. Motion position of ship 3.

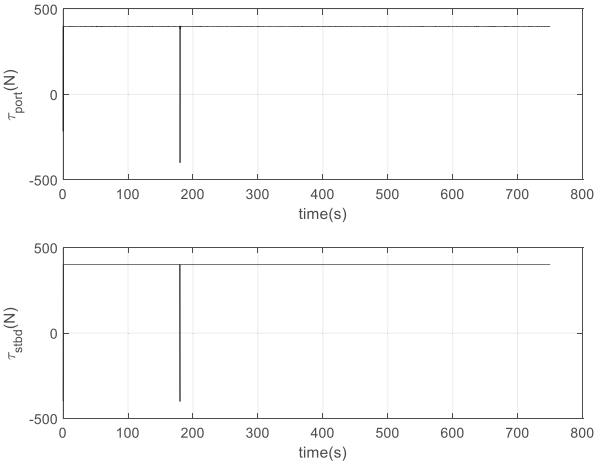

Fig. 18. Control input curve of ship 3.

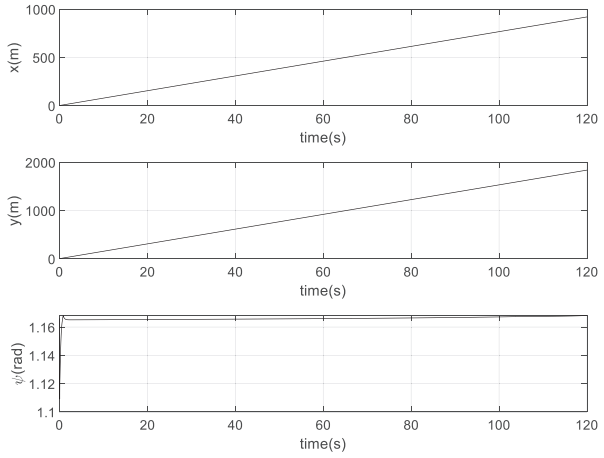

Fig. 19. Positions while berthing.

The framework of EPO for collision avoidance is illustrated in Algorithm 2.

Algorithm 2 Framework of EPO for collision avoidance

Input: parameters and encounter situations.
Output: the optimal ship turning angle for collision avoidance.
1 The initial population of EPO is generated.
2 while the termination condition is not met do
3 Calculate the fitness using Eq. (36).
4 Determine the boundary range.
5 Calculate the temperature surrounding the cluster hierarchy.
6 Calculate the distance between the emperor penguins.
7 Update the positions of the emperor penguins.
8 end while

Remark 1. The input saturation is expressed as:

$$sat(\tau)=\begin{cases}\tau_{\max}, & \tau \geq \tau_{\max}\\ \tau, & \tau_{\min}<\tau<\tau_{\max}\\ \tau_{\min}, & \tau \leq \tau_{\min}\end{cases} \tag{38}$$

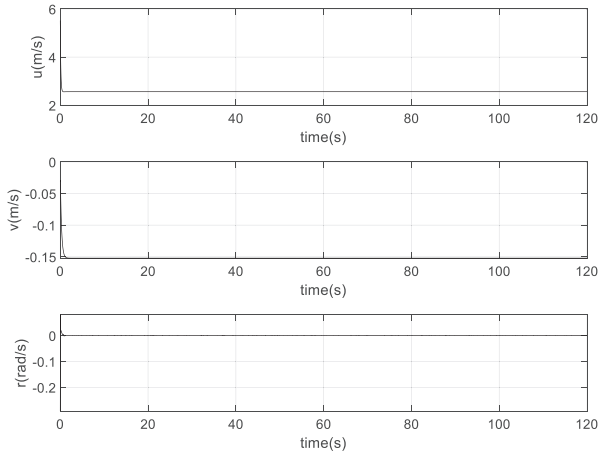

Fig. 20. Speed of the ship while berthing.

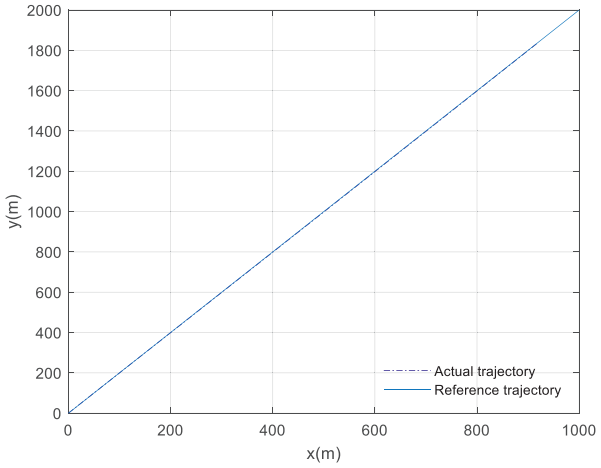

Fig. 21. Motion curve while berthing.

where $\tau_{\max}$ and $\tau_{\min}$ are the upper and lower bounds of τ, respectively.

The study presented in [39] proved that for the closed-loop system model and the saturation control law, given the initial state $\Delta x(k|k)$, positive definite matrix Ψ, weight adjustment parameters σ and $\beta > 0$, and $\gamma_1 = a\ \gamma$, if there exists $0 < a < 1$ at time k, matrices Y and Z, positive definite symmetric matrix Q and positive definite auxiliary matrix G that satisfy the following optimization problem, the control law can stabilize the closed-loop system under input saturation constraints.

The problem is given by:

$$\min_{\gamma,Y,Z,G,Q} \gamma+\beta\gamma_1 \tag{39}$$

$$s.t.\quad \gamma-\gamma_1>0$$

$$\begin{bmatrix}\chi_1 & Z\\ Z^T & G+G^T-Q\end{bmatrix}\geq 0, \chi_1 \leq (\tau_{\max}-\tau_r)^2$$

$$\begin{bmatrix}\chi_2 & Z\\ Z^T & G+G^T-Q\end{bmatrix}\geq 0, \chi_2 \leq (\tau_{\min}-\tau_r)^2$$

Table 3. Energy consumption and tracking error with different prediction horizons.

N_p	Energy	Error
3	56.3031	4.7595
4	4.9470	0.2048
5	3.1264e+04	0.1665
6	1.4775e+04	0.0265
7	4.7523e+05	0.1297
8	1.8003e+04	0.0151
10	1.3390e+06	0.1936
ours	1.3123e+04	0.0146

$$\begin{bmatrix} G+G^T-Q & (A_nG+B_nY)^T & (\Psi^{1/2}G)^T & (\sigma^{1/2}Y)^T \\ A_nG+B_nY & Q & 0 & 0 \\ \Psi^{1/2}G & 0 & \gamma_1 I & 0 \\ \sigma^{1/2}Y & 0 & 0 & \gamma_1 I \end{bmatrix} \geq 0$$

$$\begin{bmatrix} G+G^T-Q & (A_nG+B_nU)^T & (\Psi^{1/2}G)^T & (\sigma^{1/2}U)^T \\ A_nG+B_nU & Q & 0 & 0 \\ \Psi^{1/2}G & 0 & \gamma I & 0 \\ \sigma^{1/2}U & 0 & 0 & \gamma I \end{bmatrix} \geq 0$$

Remark 2. It is illegal for the ships to navigate without properly equipped sensors. As a result, the vessel may be detained by international ports. The ships should undergo regular international Port State Control (PSC) inspections where their ship-borne odometers, GPS systems, radars, and other equipment are checked to ensure compliance with international standards. The failure to meet these standards may result in the detention of the vessel. Therefore, in general, the ships are able to perceive information about surrounding obstacles with the assistance of these navigational aids, including odometers, GPS systems, and radars. In addition, in cases of poor visibility, the local maritime regulations dictate the navigation of vessels. If the approach performs under limited information about the obstacles, the selected prediction horizon is small since the recomputations will become more frequent. If the velocity of the obstacles is uncertain, the maximal velocity should be used instead for the sake of safety. The maximal velocities of yachts, container ships, and cargo ships are 20, 30, and 20 knots, respectively.

Remark 3. Compared with the algorithm proposed by Li and Zhang [16] which focused on frequency and time domain control for course keeping, this work tracks the desired trajectory and used the Matrix theory and state space.

4. Simulations

The ship model presented in [40] is used in the simulation. The main parameters of the ship are presented in Table 1.

Table 4. Energy consumption under different surge velocities for the MPC and the proposed algorithms.

u (m/s)	MPC (J)	ERNMPC (J)
8	5.74e+07	9.92e+06
7	5.04e+07	4.75e+06
6	6.48e+06	3.75e+06
5	5.99e+06	1.26e+06
4	5.30e+06	3.16e+05
3	1.72e+06	8.86e+04
2	3.32e+04	2.78e+04

4.1. Results of three ships

The considered scenario is presented in Table 2 and its visual representation is shown in Fig. 6.

The encountering situation of the three ships and the collision avoidance are shown in Fig. 7. The positional coordinate represents the position of the Automatic Identification System (AIS) antenna, which is generally located at the bridge of the ship. Note that the line presents the course of the ship.

It can be seen from Fig. 7 that the system sensor collects the status information of all the ships. It determines that the priority is for the first ship, and the priority of the second ship is higher than that of the third one. The first and second ships will maintain their reference trajectories. The third ship knows from the received prediction status that the first and second ships will keep the original track and be direct sailing ships. It decides to temporarily leave its original reference trajectory and turn 35° to the right in order to avoid collision and paves the way for the two other ships.

The position curve of ship 1 is shown in Fig. 8. Its speed, motion, and input control curves are shown in Figs. 9−11, respectively.

It can be seen from Fig. 8 that ship 1 can successfully track the reference trajectory. The tracking error approaches zero within a finite time.

It can be observed from Fig. 9 that the speed of ship 1 is within the feasible range.

It can be seen from Figs. 10 and 11 that ship 1 can successfully track a line, the overshoot and tracking error are low, and the response speed of the control system is high.

Figs. 12−14 show the position, speed, motion, and control input curves of ship 2, respectively.

It can be seen from Fig. 12 that ship 2 can successfully track the reference trajectory, and the tracking error approaches zero within a finite duration.

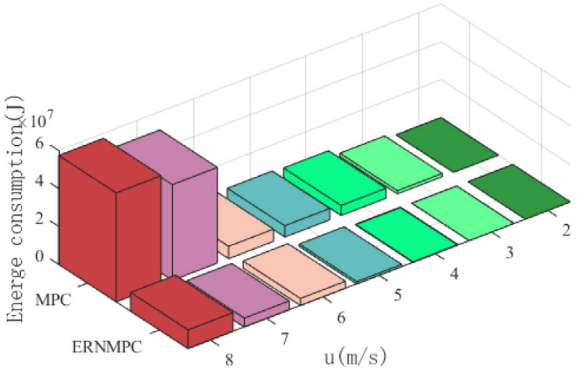

Fig. 22. Energy consumption under different surge velocities of different control algorithms.

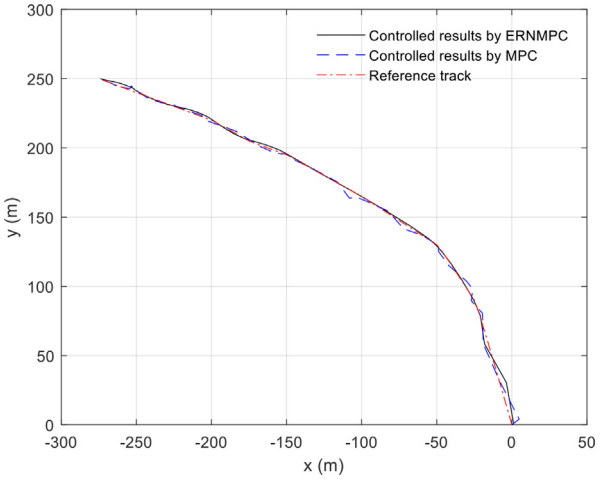

Fig. 23. Comparison of different control algorithms.

It can be observed from Fig. 13 that the speed of ship 2 is within the feasible range. It can also be seen from Fig. 14 that ship 2 can successfully track a line. In addition, the overshoot and tracking error are low, and the response speed of the control system is high.

Figs. 15–18 show the position, speed, motion, and control input curves of ship 3, respectively. Similar behaviors to those of ships 1 and 2 are observed.

It can be deduced from the results presented in Figs. 7–18 that the ship can follow the collision avoidance path in a complete and stable way. This proves the efficiency and practicability of the proposed control strategy.

4.2. Berthing test

In this test, the initial position is (0 m, 0 m), the dock is located at (1000 m, 2000 m), and the initial surge velocity is 12 knots.

The position curve of the ship is shown in Fig. 19 while its speed and motion curves are shown in Figs. 20 and 21, respectively.

It can be seen from Fig. 19 that ship 1 can successfully track the reference trajectory and the tracking error approaches zero within a finite time.

In addition, it can be observed from Fig. 20 that the speed of ship 1 is within the feasible range.

It can also be seen from Figs. 20 and 21 that it can successfully berth, the overshoot and tracking error are low, and the response speed of the control system is high.

4.3. Performance comparison

Table 3 presents the energy consumption and tracking error with different prediction horizons.

Table 5. Comparison of cost.

Algorithms	Best	Worst	Average
PSO	146.21	151.46	149.30
EPO	138.18	127.25	130.59
Sobol-EPO	113.86	116.15	114.24

Table 3 shows the sensitivity of the energy consumption and tracking error with respect to the chosen prediction horizon. It can be seen that with large fixed prediction horizon, the energy consumption is high, while in the case of small fixed prediction horizon, the tracking error is high. Therefore, the adaptive prediction horizon based energy-saving robust nonlinear model predictive control can outperform existing algorithms with fixed prediction horizons. In other words, it is able to obtain a balance between the energy consumption and the tracking error.

The proposed algorithm is then compared with the MPC method. The average energy consumption of the two methods, under different surge velocities, is presented in Table 4. A graphical representation is also shown in Fig. 22.

Moreover, the tracking curves of different control algorithms are shown in Fig. 23, where the blue dashed line represents the tracking path controlled by MPC, while the red solid line represents the tacking path controlled by ERNMPC. It can be seen that the control strategy is significantly improved. MPC shows a greater overshoot and tracking error, while ERNMPC can perform tracking within a smaller overshoot, which results in reducing the energy usage. Compared with the MPC, ERNMPC has higher response speed, smaller overshoot, and shorter system adjustment time.

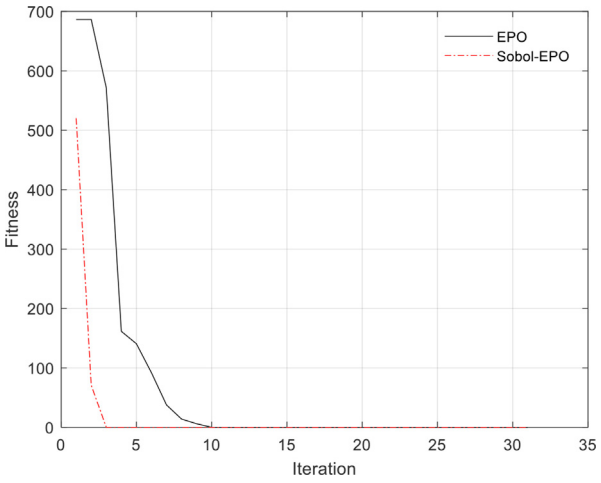

Fig. 24. Comparison of different optimization algorithms.

The comparison of cost is listed in Table 5.

The comparison of different optimization algorithms is shown in Fig. 24.

The results in Table 5 and Fig. 24 demonstrate the feasibility and superiority of the Sobol-EPO algorithm. The Sobol-EPO outperforms the EPO in terms of computational load.

4.4. Discussion

The energy consumption of the unmanned surface ship is different in several wind directions. It can be seen from Table 4 that the consumed energy increases with the speed where the hydrostatic resistance is gradually increasing. More energy is consumed to overcome the hydrostatic resistance. The saved energy is greater than the work done by the increased hydrostatic resistance, and thus an appropriate speed should be selected in the environment for different strengths.

It is also deduced from Table 4 that, when the intensity and direction of environmental load are different, the saved energy is also different. The energy consumed by the unmanned surface ship when it moves at different speeds and in different environmental intensities, is also analyzed. The reasons for the different amounts of consumed energy in the case of different speeds are then determined.

In collision avoidance navigation activities, communication is conducted on collision avoidance information, fusion interaction, cognitive mechanism, analytic methods, navigation decision, and intelligent control. The system design significantly affects the traditional ship-shore relationship, navigation in the waterway, and collision avoidance in complex waters, as well as the organization and collaboration of ship traffic.

5. Conclusion

In this paper, an adaptive prediction horizon based energy-saving robust model predictive control, referred to as APHERNMPC, is designed for underactuated USVs to deal with the actual control and state constraints during berthing. The existing objective function of the model predictive control is improved. The energy consumption is constructed and considered as one of the objective functions in the NMPC framework. Based on these constraints and requirements, a novel actual control and state constraint, during the berthing framework algorithm, is proposed. At each sampling time, the finite time domain optimal control problem is established based on the nonlinear ship maneuverability. Different berthing methods are implemented by robust model predictive control under different disturbances, including the direct berthing and the turning round berthing method. The close association between ship maneuvering control and energy consumption is performed in the control strategy. The proposed system is tested for ship trajectory tracking control with the presence of wind and current disturbances. In addition, this paper discusses the energy consumed by the USV when it moves at different speeds in different environmental intensities. It also discusses the reasons for the differences in energy consumption when the speed varies.

In future work, we aim at improving the intelligent energy-saving control method to deal with automatic berthing. Reducing the actuator chatter and improving the heading stability are also of our interest.

Conflict of interest

There is no conflict of interest.

Appendix A

The proof of Eq. (29) is illustrated below.

X_e can be expressed as follow:

$$X_e = \begin{bmatrix} \cos\Psi & \sin\Psi & 0 \\ -\sin\Psi & \cos\Psi & 0 \\ 0 & 0 & 1 \\ 1 & 0 & 0 \\ 0 & 1 & 0 \\ 0 & 0 & 1 \end{bmatrix} \begin{bmatrix} x - x_d \\ y - y_d \\ \Psi - \Psi_d \\ u - u_d \\ v - v_d \\ r - r_d \end{bmatrix} = \begin{bmatrix} \cos\Psi(x - x_d) + \sin\Psi(y - y_d) \\ -\sin\Psi(x - x_d) + \cos\Psi(y - y_d) \\ \Psi - \Psi_d \\ u - u_d \\ v - v_d \\ r - r_d \end{bmatrix} \tag{40}$$

By differentiating Ψ_e, one can obtain:

$$\dot{\Psi}_e = \dot{\Psi} - \dot{\Psi}_d = r - r_d = r_e \tag{41}$$

In addition, by differentiating ue, we can obtain

$$\begin{aligned} \dot{u}_e &= \dot{u} - \dot{u}_d \\ &= \frac{m_{22}}{m_{11}}(vr - u_d r_d) - \frac{d_{11}}{m_{11}}u_e + \frac{1}{m_{11}}\tilde{\tau}_u \\ &= \frac{m_{22}}{m_{11}}(vr_e + vr_d - u_d r_d) - \frac{d_{11}}{m_{11}}u_e + \frac{1}{m_{11}}\tilde{\tau}_u \\ &= \frac{m_{22}}{m_{11}}(v_e r_e + v_d r_e + v_e r_d) - \frac{d_{11}}{m_{11}}u_e + \frac{1}{m_{11}}\tilde{\tau}_u \end{aligned} \tag{42}$$

where τud is the desired control input along the surging direction. Then, the error of control input along the surging direction is expressed as follow:

$$\tilde{\tau}_u = \tau_u - \tau_{ud} \tag{43}$$

Similarly, by differentiating *ve* and *re*, one can get the following equations:

$$\begin{aligned}\dot{v}_e &= \dot{v} - \dot{v}_d = -\frac{m_{11}}{m_{22}}(ur - u_d r_d) - \frac{d_{22}}{m_{22}}v_e \\ &= -\frac{m_{11}}{m_{22}}(u_e r_e + u_e r_d + u_d r_e) - \frac{d_{22}}{m_{22}}v_e\end{aligned} \tag{44}$$

$$\begin{aligned}\dot{r}_e &= \dot{r} - \dot{r}_d \\ &= \frac{m_{11} - m_{22}}{m_{33}}(uv - u_d v_d) - \frac{d_{33}}{m_{33}}r_e + \frac{1}{m_{33}}\tilde{\tau}_r \\ &= \frac{m_{11} - m_{22}}{m_{33}}(u_e v_e + u_e v_d + u_d v_e) - \frac{d_{33}r_e}{m_{33}} + \frac{\tilde{\tau}_r}{m_{33}}\end{aligned} \tag{45}$$

where τrd is the desired control input along the yawing direction. The error of control input along the surge direction is

$$\tilde{\tau}_r = \tau_r - \tau_{rd} \tag{46}$$

In addition, by differentiating *xe*, one can obtain:

$$\begin{aligned}&\dot{x}_e = \cos\Psi(\dot{x} - \dot{x}_d) - r\sin\Psi x_e + \\ &\sin\Psi(\dot{y} - \dot{y}_d) + r\cos\Psi y_e \\ &= \cos\Psi(u\cos\Psi - v\sin\Psi - u_d\cos\Psi_d + \\ &v_d\sin\Psi_d) - r\sin\Psi x_e + r\cos\Psi y_e + \sin\Psi \cdot \\ &(u\sin\Psi + v\cos\Psi - u_d\sin\Psi_d - v_d\cos\Psi_d) \\ &= u - u_d\cos\Psi_e - v_d\sin\Psi_e \\ &-r\sin\Psi x_e + r\cos\Psi y_e \\ &= u_e + (1 - \cos\Psi_e)u_d - v_d\sin\Psi_e \\ &-r\sin\Psi x_e + r\cos\Psi y_e\end{aligned} \tag{47}$$

Referring to Eq. (40), where ye = -sinΨxe + cosΨye, one can write:

$$\sin\Psi x_e = (\cos\Psi - 1)y_e \tag{48}$$

By substituting Eq. (48) into Eq. (47), the new expression of the differentiation of *xe* is expressed as follow:

$$\begin{aligned}\dot{x}_e &= u_e + (1 - \cos\Psi_e)u_d - v_d\sin\Psi_e + ry_e \\ &= r_e y_e + r_d y_e + u_e + (1 - \cos\Psi_e)u_d - v_d\sin\Psi_e\end{aligned} \tag{49}$$

By differentiating *ye*, we can obtain

$$\begin{aligned}&\dot{y}_e = -r\cos\Psi x_e - r\sin\Psi y_e - \sin\Psi(\dot{x} - x_d) + \cos\Psi(\dot{y} - \dot{y}_d) \\ &= -r\cos\Psi x_e - r\sin\Psi y_e - \sin\Psi(u\cos\Psi - \\ &v\sin\Psi - u_d\cos\Psi_d + v_d\sin\Psi_d) + \cos\Psi \cdot \\ &(u\sin\Psi + v\cos\Psi - u_d\sin\Psi_d - v_d\cos\Psi_d) \\ &= -r\cos\Psi x_e - r\sin\Psi y_e + v + \\ &u_d\sin\Psi_e - v_d\cos\Psi_e \\ &= -r\cos\Psi x_e - r\sin\Psi y_e + v_e + \\ &\sin\Psi_e u_d + (1 - \cos\Psi_e)v_d\end{aligned} \tag{50}$$

Referring to Eq. (40), where x_e = cosΨx_e + sinΨy_e in Eq. (34), one can write:

$$\sin\Psi y_e = (1 - \cos\Psi)x_e \tag{51}$$

Substituting Equation (51) into Equation (50) results in:

$$\begin{aligned}&\dot{y}_e = -r\cos\Psi x_e - r\sin\Psi y_e + v_e \\ &+\sin\Psi_e u_d + (1 - \cos\Psi_e)v_d \\ &= -ry_e + v_e + \sin\Psi_e u_d + (1 - \cos\Psi_e)v_d \\ &= -r_e y_e - r_d y_e + v_e + \sin\Psi_e u_d + (1 - \cos\Psi_e)v_d\end{aligned} \tag{52}$$

Thus, the error dynamics can be written as Eq. (29).

Appendix B

The proof of Theorem 1 is illustrated below.

Proof. The cost function is computed as below:

$$\begin{aligned}J_{k+1} &= P_{N_p}(f(X_e, U)) + \sum_{i=1}^{N_p - 1}\left(\frac{i}{N_p}\right)^n P_{i+1} \\ &= P_{N_p}(f(X_e, U)) + \sum_{i=2}^{N_p}\left(\frac{i-1}{N_p}\right)^n P_i \\ &= P_{N_p}(f(X_e, U)) + \sum_{i=2}^{N_p}\left(\frac{i-1}{i}\right)^n\left(\frac{i}{N_p}\right)^n P_i \\ &= P_{N_p}(f(X_e, U)) + \sum_{i=2}^{N_p}\left(\frac{i}{N_p}\right)^n P_i \\ &+ \sum_{i=2}^{N_p}\left[\left(\frac{i-1}{i}\right)^n - 1\right]\left(\frac{i}{N_p}\right)^n P_i\end{aligned} \tag{53}$$

One can get the following equations:

$$\sum_{i=2}^{N_p}\left(\frac{i}{N_p}\right)^n P_i = J_k - \frac{1}{N_p^m}P_k \tag{54}$$

Substituting Eq. (54) into Eq. (53) gives:

$$\begin{aligned}J_{k+1} = P_{N_p}(f(X_e, U)) + J_k - \frac{1}{N_p^m}P_k - \sum_{i=2}^{N_p}\Bigg[1 \\ - \left(\frac{i-1}{i}\right)^n\Bigg]\left(\frac{i}{N_p}\right)^n P_i\end{aligned} \tag{55}$$

Denote:

$$\lambda = 1 - \left(\frac{N_p - 1}{N_p}\right)^n \le 1 - \left(\frac{j-1}{j}\right)^n, j \le N_p \tag{56}$$

Substituting Eq. (56) into Eq. (55) gives:

$$\begin{aligned}J_{k+1} &= J_k + P_{N_p}(f(X_e, U)) - \lambda\sum_{i=2}^{N_p}\left(\frac{i}{N_p}\right)^n P_i - \frac{1}{N_p^m}P_k \\ &\le J_k + P_{N_p}(f(X_e, U)) - \lambda P_{N_p} - \frac{1}{N_p^m}P_k\end{aligned} \tag{57}$$

Substituting Eq. (34) into Eq. (57) gives:

$$J_{k+1} \le J_k + P_{N_p} - \beta(X_e) - \lambda P_{N_p} - \frac{1}{N_p^m} P_k = J_k - \frac{1}{N_p^m} P_k + (1-\lambda) P_{N_p} - \beta(X_e) \tag{58}$$

Substituting Eq. (35) into Eq. (58) gives:

$$J_{k+1} \le J_k - \frac{1}{N_p^m} P_k - (\lambda + \mu - 1) P_{N_p} \tag{59}$$

Since $\lim_{n\to\infty} 1 - \left(\frac{N_p-1}{N_p}\right)^n = 1$, there is a finite n such that $\lambda + \mu - 1 \ge 0$.
Eq. (59) gives

$$J_{k+1} \le J_k \tag{60}$$

The above expression indicates that J_k is bounded. It demonstrates that the control sequence satisfies the optimization problem and ensures that the objective function value is bounded, making it a feasible solution.
When $X_e = 0$, the input is a feasible solution to the optimization problem, corresponding to $J = 0$. From equations (32) and (33), it can be deduced that $J_k \ge 0$. From equation (60), it can be observed that J_k is monotonically decreasing and attains its minimum value at $X_e = 0$. Hence, it can be concluded that J_k is continuous $X_e = 0$. Thus, J_k is a Lyapunov function for the closed-loop system. From Lemma 1, the system is asymptotically stable.

Acknowledgement

This work was supported in part by the National Natural Science Foundation of China (No. 52201411) and Natural Science Foundation of Fujian Province (No. 2021J01819, 2023I0019).

References

[1] Liu Q, Li T, Shan Q, Yu R, Gao X. Virtual guide automatic berthing control of marine ships based on heuristic dynamic programming iteration method. Neurocomputing 2021;437:289−99.
[2] Zhang Q, Zhu G, Hu X, Yang R. Adaptive neural network auto-berthing control of marine ships. Ocean Eng 2019;177:40−8.
[3] Xue H, Ou Y. A novel asymmetric barrier Lyapunov function-based fixed-time ship berthing control under multiple state constraints. Ocean Eng 2023;281:114756.
[4] Li S, Liu J, Negenborn RR, Wu Q. Automatic docking for underactuated ships based on multi-objective nonlinear model predictive control. IEEE Access 2020;8:70044−57.
[5] Y. Zhang, M. Zhang, Q. Zhang, "Auto-berthing control of marine surface vehicle based on concise backstepping," IEEE Access, vol. 8, pp. ,197059-197067 2020.
[6] Wang L, Li S, Liu J, Wu Q, Negenborn RR. Ship docking and undocking control with adaptive-mutation beetle swarm prediction algorithm. Ocean Eng 2022;251. https://doi.org/10.1016/j.oceaneng.2022.111021. Art. no. 111021.
[7] Feng G, Han Y, Li SE, Xu S, Dang D. Accurate pseudo-spectral optimization of nonlinear model predictive control for high-performance motion planning. IEEE Transactions on Intelligent Vehicles 2022. https://doi.org/10.1109/TIV.2022.3153633.
[8] Kong S, Sun J, Wang J, Zhou Z, Shao J, Yu J. Piecewise compensation model predictive governor combined with conditional disturbance negation for underactuated AUV Tracking control. IEEE Trans Ind Electron 2022. https://doi.org/10.1109/TIE.2022.3194637.
[9] Liang H, Li H, Xu D. Nonlinear model predictive trajectory tracking control of underactuated marine vehicles: Theory and experiment. IEEE Trans Ind Electron 2021;68(5):4238−48.
[10] Yan Z, Wang J. Model predictive control for tracking of underactuated vessels based on recurrent neural networks. IEEE J Ocean Eng 2012;37(4):717−26.
[11] Wang L, Li S, Liu J, Wu Q. Data-driven model identification and predictive control for path-following of underactuated ships with unknown dynamics. Int J Nav Archit Ocean Eng 2022;14:100445. https://doi.org/10.1016/j.ijnaoe.2022.100445.
[12] Sandeepkumar R, Rajendran S, Mohan R, Pascoal A. A unified ship manoeuvring model with a nonlinear model predictive controller for path following in regular waves. Ocean Eng 2022;243. https://doi.org/10.1016/j.oceaneng.2021.110165. Art. no. 110165.
[13] Kucukdemiral IB, Cakici F, Yazici H. A model predictive vertical motion control of a passenger ship. Ocean Eng 2019;186. https://doi.org/10.1016/j.oceaneng.2019.06.005. Art. no. 106100.
[14] Liu C, Hu Q, Wang X, Yin J. Event-triggered-based nonlinear model predictive control for trajectory tracking of underactuated ship with multi-obstacle avoidance. Ocean Eng 2022;253. https://doi.org/10.1016/j.oceaneng.2022.111278. Art. no. 111278.
[15] Yang H, Deng F, He Y, Jiao D, Han Z. Robust nonlinear model predictive control for reference tracking of dynamic positioning ships based on nonlinear disturbance observer. Ocean Eng 2020;215. https://doi.org/10.1016/j.oceaneng.2020.107885. Art. no. 107885.
[16] G. Li, X. Zhang. Green energy-saving robust control for ship course-keeping system based on nonlinear switching feedback. Ocean Eng 268, 15 January 2023, 113462.
[17] Haseltalab A, Negenborn RR. Model predictive maneuvering control and energy management for allelectric autonomous ships. Appl Energy 2019;251. https://doi.org/10.1016/j.apenergy.2019.113308. Art. no. 113308.
[18] Min B, Zhang X, Wang Q. Energy saving of course keeping for ships using CGSA and nonlinear decoration. IEEE Access 2020;8:141622−31.
[19] Zhang Y, Li S, Liu X. Adaptive near-optimal control of uncertain systems with application to underactuated surface vessels. IEEE Trans Control Syst Technol 2018;26(4):1204−18.
[20] Zhang S, Wang J, Wen X, Zhao M, Zhang C, Cong X. "An energy-saving control method for path following of an unmanned surface vehicle in wave field," Conference: 2018 International Symposium in Sensing and Instrumentation in IoT Era (ISSI). 2018. https://doi.org/10.1109/ISSI.2018.8538200.
[21] Osman Ü, Nuri A. Smart Sounding Table Using Adaptive Neuro-Fuzzy Inference System. J Mar Sci Technol 2023;31:273−82.
[22] Dhiman G, Kumar V. Emperor penguin optimizer: A bio-inspired algorithm for engineering problems. Knowl Base Syst 2018;159:20−50.
[23] Baliarsingh SK, Vipsita S, Muhammad K, Bakshi S. Analysis of high-dimensional biomedical data using an evolutionary multi-objective emperor penguin optimizer. Swarm Evol Comput 2019;48:262−73.
[24] Ganesh S, Elangovan P, Jimreeves JSR, Subramaniyan J. Modified emperor penguin optimizer for optimal allocation of energy storage system and phasor measurement units. Mater Today Proc 2021;45:7871−5. Part 9.

[25] Khalid OW, Isa NAM, Sakim HAM. Emperor penguin optimizer: A comprehensive review based on state-of-the-art meta-heuristic algorithms. Alex Eng J 2022. https://doi.org/10.1016/j.aej.2022.08.013.
[26] Khan AI, Alghamdi ASA, Abushark YB, Alsolami F, Almalawi A, Ali AM. Recycling waste classification using emperor penguin optimizer with deep learning model for bioenergy production. Chemosphere 2022;307:136044. Part 3.
[27] X. Lu, Y. Yang, P. Wang, Y. Fan, F. Yu, N. Zafetti, "A new converged Emperor Penguin Optimizer for biding strategy in a day-ahead deregulated market clearing price: A case study in China," Energy, vol. 227, Art. no. 120386, 2021, doi: 10.1016/j.energy.2021.120386.
[28] H. Kaur, A. Rai, S. S. Bhatia, G. Dhiman, "MOEPO: A novel multi-objective emperor penguin optimizer for global optimization: special application in ranking of cloud service providers," Engineering Applications of Artificial Intelligence, vol. vol. 96, Art. no. 104008, 2020, doi: 10.1016/j.engappai.2020.104008.
[29] Dhiman G, Oliva D, Kaur A, Singh KK, Vimal S, Sharma A, Cengiz K, BEPO. A novel binary emperor penguin optimizer for automatic feature selection. Knowl Base Syst 2021;211. Art. no. 106560.
[30] Xing Z. An improved emperor penguin optimization based multilevel thresholding for color image segmentation. Knowl Base Syst 2020;194. https://doi.org/10.1016/j.knosys.2020.105570. Art. no. 105570.
[31] Xue H. A quasi-reflection based SC-PSO for ship path planning with grounding avoidance. Ocean Eng 2022;247:110772.
[32] Xue H, Li S. Predefined-time Neural Sliding Mode Control based Trajectory Tracking of Autonomous Surface Vehicle. Journal of Marine Science and Technology-Taiwan 2023;31(3):193−204.
[33] Li Y, Peng Y, Zheng J. Intelligent ship collision avoidance model integrating human thinking experience. Ocean Eng 2023;286. Art. no. 115510.
[34] Fossen TI. Handbook of marine craft hydrodynamics and motion control. 1st. Edition. Wiley; 2011.
[35] Chen H. "Model predictive control". Beijing: Science Press; 2013.
[36] Xu Y. Research on collision avoidance control methods for multiple dynamic positioning ships. Harbin Engineering University; 2018.
[37] H. Xue, T. Chai, "Risk assessment based on KDE of ship collision candidates for ship routing waterway," doi: 10.5957/JOSR.12210045.
[38] Xue H, Qian K. Ship collision avoidance based on brain storm optimization near offshore wind farm. Ocean Eng 2023;268:2023. Art. no. 113433.
[39] Hu C, Ren Y, Xie Q. Input Saturation Control Based on RMPC for Hypersonic Vehicles. Aerospace Control 2016;34(2):20−26+30.
[40] Wooa J, Parka J, Yu C, Kim N. Dynamic model identification of unmanned surface vehicles using deep learning network. Appl Ocean Res 2018;78:123−33.